Supporting Information

Flexible and Stable Piezoelectric Nanogenerators Based on Monoclinic Phase $CsPbBr_3$ Perovskite Nanocrystals

Jingkun Xu, Yechen Zhou, Hao Jiang,* Kaiyan Zhu, Ying Wan, Min Lai, Shuhong Xu**

J. Xu, Y. Zhou, K. Zhu, Prof. M. Lai, Prof. Y. Wan,
School of Physics and Optoelectronic Engineering, Nanjing University of Information Science & Technology, Nanjing 210044, China
Email: xjk@nuist.edu.cn

H. Jiang
Smart Manufacturing Thrust, Systems Hub, The Hong Kong University of Science and Technology, Guangzhou 511458, China
Email: hjiang302@connect.hkust-gz.edu.cn

Prof. S. Xu
Advanced Photonics Center, School of Electronic Science and Engineering, Southeast University, Nanjing, 210096, P. R. China
Email: xush@seu.edu.cn

Experimental section

Materials: $PbBr_2$ (lead (II) bromide 99%, Aladdin), CsAC (Cesium acetate 99.9%, Aladdin), n-octylamine(≥99%, Aladdin), oleic acid (OA) (90%, Alfa Aesar), N, N-dimethylformamide (DMF) (99.5%, Kelong), n-hexane (97%, Kelong), acetone (99.5%, Sinopharm Chemical Reagent Co., Ltd), polydimethylsiloxane (PDMS, Dow Corning Sylgard 184). All the reagents were purchased and used without any treatment.

Synthesis of $CsPbBr_3$ perovskite nanocrystals: Colloidal $CsPbBr_3$ perovskite nanocrystals were synthesized according to the literature.[12] In the synthesis procedure: the Cs-precursor was prepared via dissolving 1 mmol CsAC in 1 mL DMF; the Pb-precursor was prepared via dissolving 1 mmol $PbBr_2$ in 1mL DMF. 6 ml OA and 0.8 ml n-octylamine in 30 mL n-hexane. Then the precursor solution was added dropwise into the above solution. Along with the mixing, emulsion was formed and the color of solution turned from clear to slight white. Demulsion and purification process were via adding 20 mL acetone into the above crude solution. Then the mixture was centrifugated at 8000 rpm for 10 min to obtain precipitates and then redissolved in 2 mL n-hexane for the fabrication of composite film.

Fabrication of $CsPbBr_3$ NCs @ PDMS composite film and PNGs: The composite film was prepared via dropping the above 2 mL $CsPbBr_3$ NCs n-hexane solution into the 10 g PDMS matrix. After stirring 30 minutes, a curing agent was added into the mixture with a weight ratio of 1:10 with the PDMS matrix. Then the as-prepared solution was drop-casted onto PET/ITO substrate. Before curing the film at 120 ℃ for 2 hours, the degassing was needed inside a vacuum chamber for few hours to remove the residual bubbles. A copper electrode was attached to the top surface of the $CsPbBr_3$ @ PDMS film as the top electrode. To improve the device performance, the dipoles need to be aligned at a high electrical poling voltage of 6.0 kV for 2-3 hours operated in dry atmosphere at room temperature. The size of the fabricated devices was 4 cm×9 cm with a 2 cm×4 cm active area.

Characterization and measurements: UV–vis absorption spectra were recorded with a Shimadzu 3600 UV–vis near-infrared spectrophotometer. Photoluminescence (PL) spectra were recorded with the Shimadzu RF-5301 PC spectrofluorometer. X-ray powder diffraction (XRD) investigation was carried out by Bruker d8 advance. X-ray photoelectron spectroscopy (XPS) was performed using a PHI550 spectrometer with Mg kα excitation (1253.6 eV). Transmission electron microscopy (TEM) was recorded by a JEM-2100 electron microscope

with an acceleration voltage of 200 kV. To measure the electrical output from the PENGs, an electrodynamic shaker system (ET-140, Lab works Inc.) was used to create periodic mechanical excitation. The applied mass was 210 g at an acceleration of 2 G. The calculated force (F) was 4.2 N based on the equation of F = MA. If not specified, all of the measurements were tested at a force of 4.2 N. By controlling the mass loading, the electromechanical response along with different loadings could be analyzed. The generated output voltage from the device was recorded by a digital oscilloscope (Tektronix 2004C) with a 100 MΩ probe, and the short-circuit current was measured by a low-noise current preamplifier (SR570, Stanford Research Systems, Inc.). To remove any external artifact signals, the measurement was performed on an electrically grounded platform and turning off nearby mechanical machinery in the laboratory.

The **energy conversion efficiency** is calculated using the reported method.[8]

The energy conversion efficiency of the $CsPbBr_3$ NCs @ PDMS composite PNG is estimated as the ratio $\eta = E_e/E_s$ between the mechanical strain energy E_s and the average energy storage in capacitor E_e for one cycle of mechanical compression. The mechanical strain energy E_s is expressed as $E_s = 1/2YAL\sigma^2$, where A is the active area of 2×4 cm^2, L is the composite thickness of 800 μm, σ is the strain and Y is the Young's modulus of the material which is estimated to be about 0.63 GPa. And the strain σ is estimated about 0.0083% at 5.25 KPa compression according to the equation of $\sigma = P/Y$, P is the applied pressure. The mechanical strain energy is found to be about 13.8 nJ. And the energy storages in the capacitor of 1 μF is calculated by $E_e = 1/2CV^2$, which is about 4.5 μJ for the charging time of 1500 cycling times during 50 s. (Here, testing conditions were 30 Hz and an applied force of 4.2 N. The 1 μF capacitor can be charged to 3 V in 50 s.) As a result, the energy conversion efficiency of our PNG is about 21.7%.

COMSOL simulation details:

The COMSOL simulation model is structured with a mesh section to define the discretization of the geometry, ensuring accurate solutions across the domain. The mesh is configured as a free triangular mesh, with a regular element size for adequate resolution and computational efficiency. It contains two main materials: PDMS for flexible applications, $CsPbBr_3$ perovskite materials with specific piezoelectric and dielectric properties. The geometry consists of a 2D square region (100 nm * 100 nm) containing a periodic array of circular inclusions. Each circle represents a $CsPbBr_3$ nanocrystal within the host material. The physics setup includes both solid mechanics and electrostatics modules. The solid mechanics module is used to apply mechanical

boundary conditions, including fixed constraints and boundary loads, allowing for stress and strain analysis within the composite structure. The electrostatics module incorporates dielectric properties, where the relative permittivity equation is defined to simulate the material's response to an electric field.

In the COMSOL simulation setup, the $CsPbBr_3$ material (mat1) is characterized by a density (ρ) of 5680 kg/m³ and an anisotropic relative permittivity tensor, with values for (ε_{11}, ε_{22}, ε_{33}) specified as (8.5446, 8.5446, 10.204). The strain-charge form includes elastic constants in Voigt notation (e.g., s_{E11}, s_{E12}) with values given in units of 1/Pa, as well as piezoelectric coupling coefficients (d_{E11}, d_{E22}, etc.) measured in C/N, capturing the material's response to both mechanical and electrical stimuli. For the PDMS material (mat2), a density of 1780 kg/m³ is defined, alongside a relative permittivity tensor with (ε_{11}, ε_{22}, ε_{33}) values of (7.4, 9.3, 7.6), reflecting its dielectric properties. Both strain-charge and stress-charge forms are included, with elastic constants provided in units of Pa and piezoelectric properties specified to illustrate the material's coupled mechanical and electrical response. This comprehensive parameterization enables accurate modeling of both materials' behaviors under complex loading conditions.

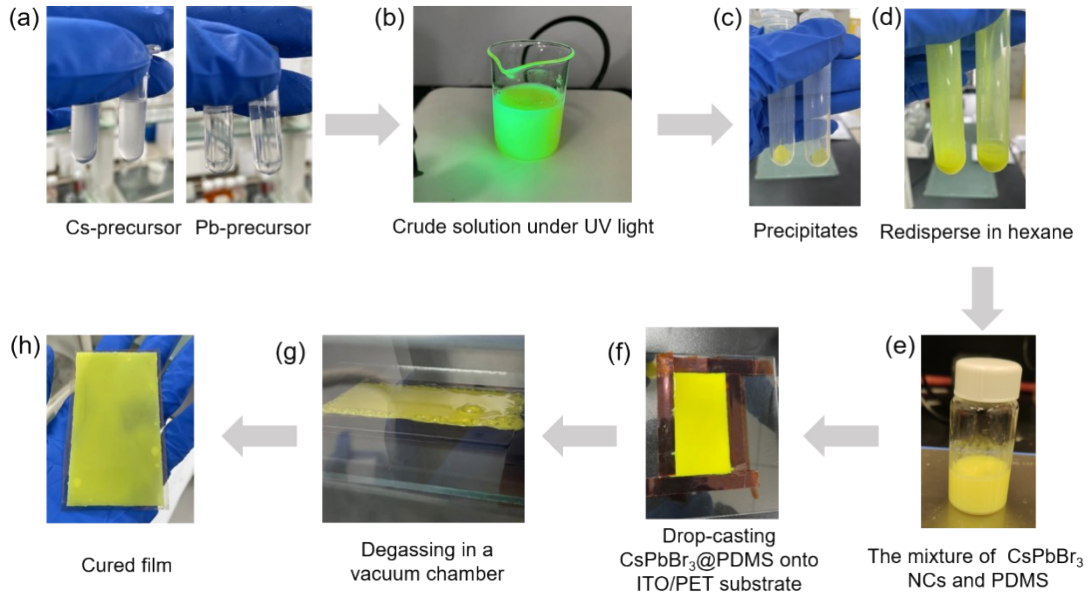

Figure S1. A photograph of the object corresponding to each step in the synthesis of $CsPbBr_3$ NCs (a-d) and the preparation of $CsPbBr_3$@PDMS composite film (e-h).

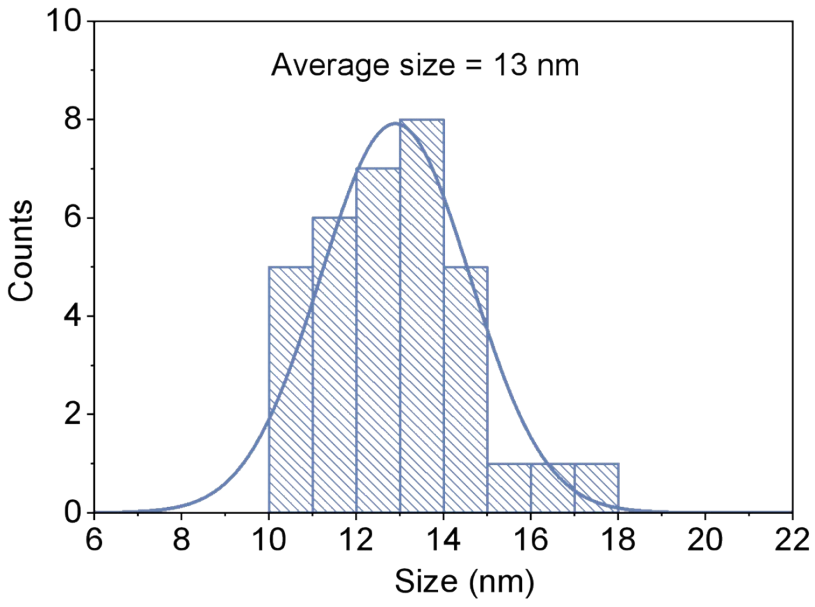

Figure S2. Size distribution histogram of the $CsPbBr_3$ NCs.

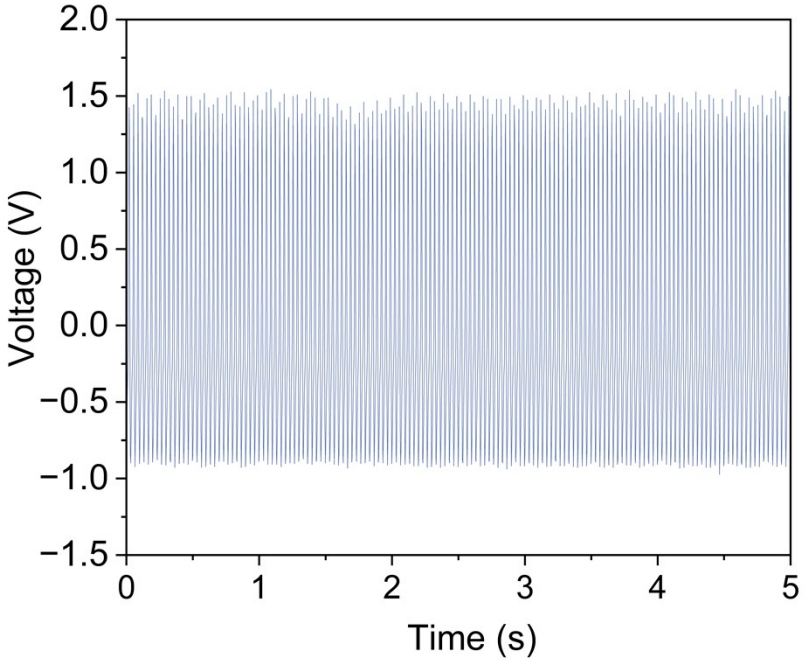

Figure S3. The voltage output of $PbBr_2$-based device.

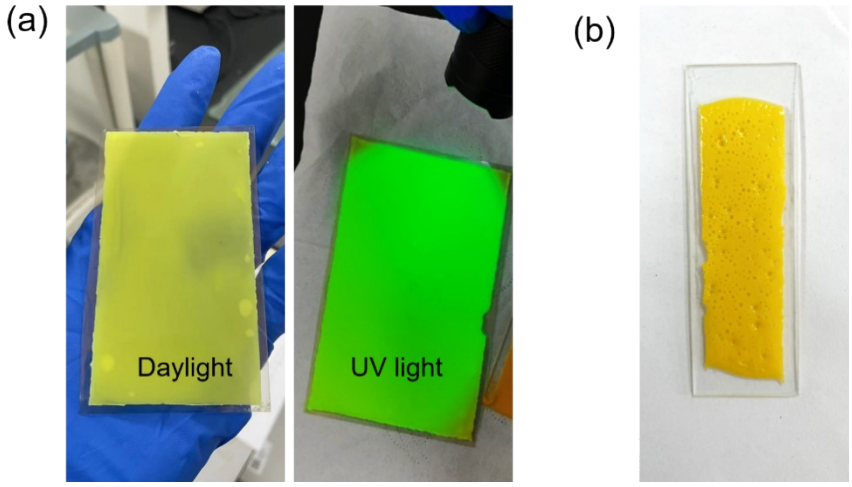

Figure S4. (a) Photographs of $CsPbBr_3$ NCs @ PDMS composite film with vacuum degassing process, taken under daylight and UV lamp. (b) Photographs of $CsPbBr_3$ NCs @ PDMS composite film without vacuum degassing process, taken under daylight.

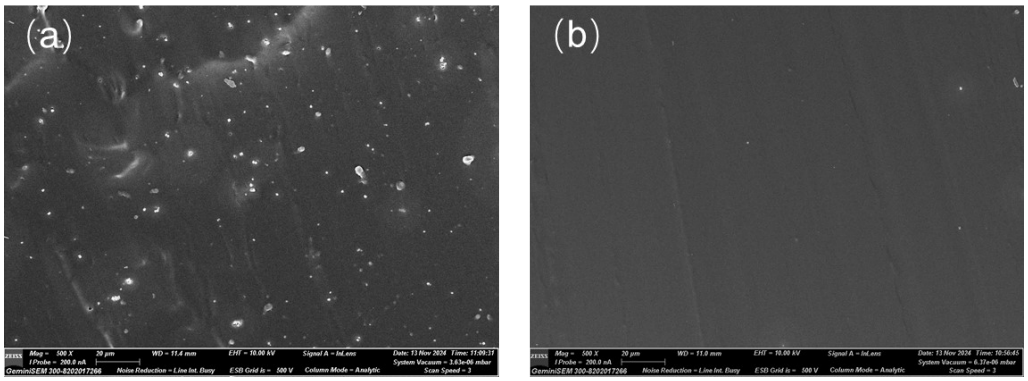

Figure S5. SEM images of (a) $CsPbBr_3$ NCs @ PDMS composite film and (b) pure PDMS film on PET/ITO substrate in cross-sectional view.

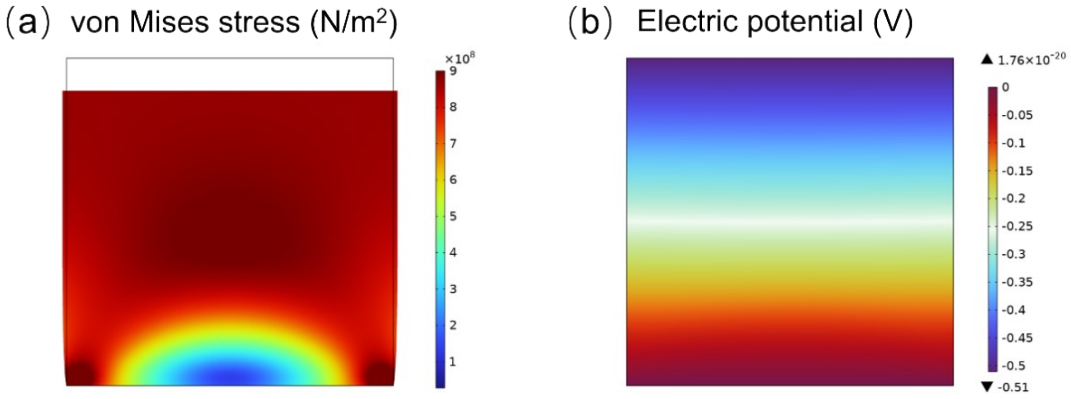

Figure S6. (a) the strain distribution of pure PDMS matrix. (b) the piezopotential distribution of pure PDMS matrix.

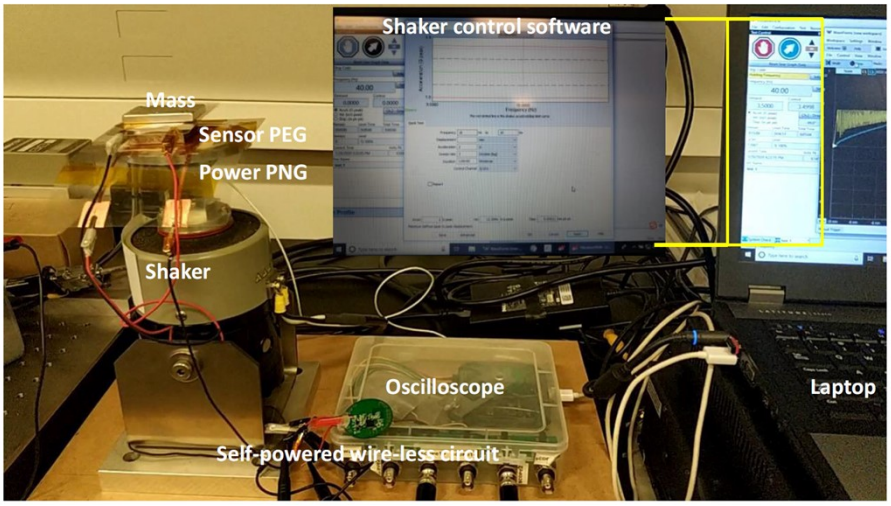

Figure S7. A photograph of the PNG characterization set-up, including a mass, PNG, electrodynamic shaker, oscilloscope, shaker controller and the control software.

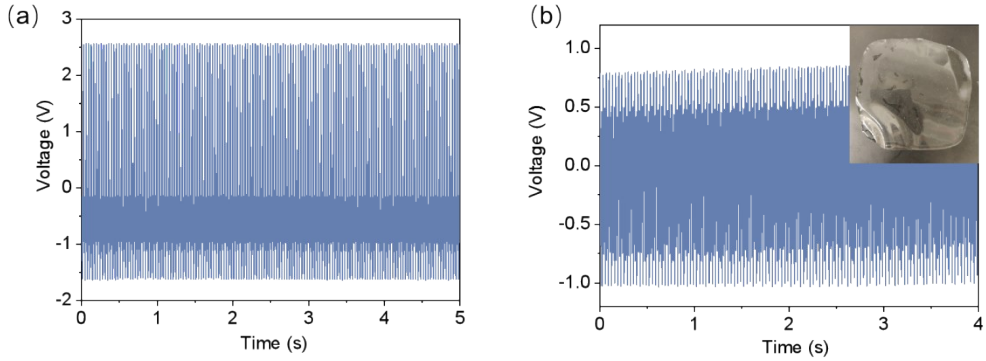

Figure S8. (a) Piezoelectric output voltage from $CsPbBr_3$-PDMS composite nanogenerator without poling treatment. (b) Output voltage from only PDMS based device under mechanical compression. Inset is the photograph of pure PDMS film.

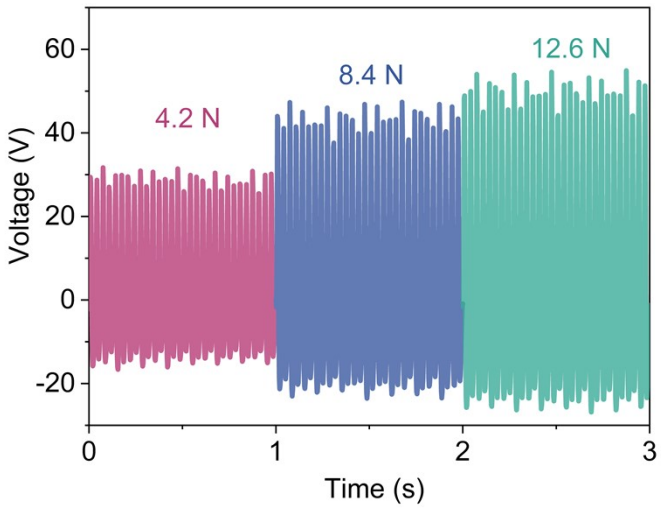

Figure S9. The output voltage of PNG measured at applied force from 4.2 to 12.6 N.

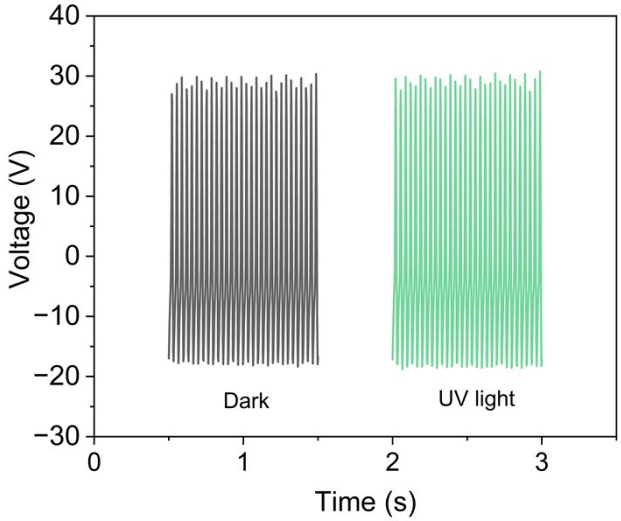

Figure S10. The output voltage of PNG measured in the dark and under 365 nm ultraviolet radiation.

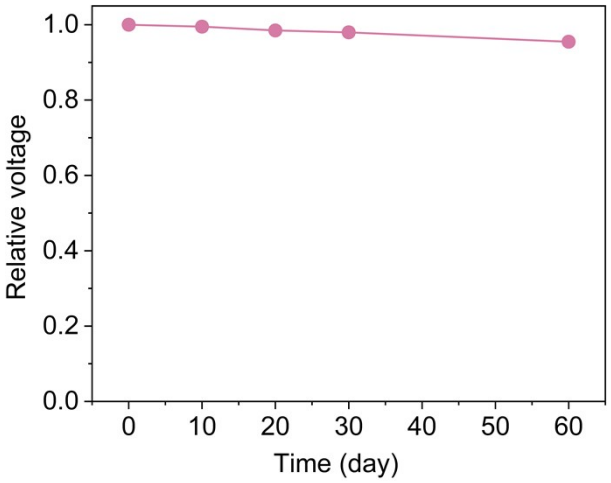

Figure S11. The stability test of PNG. The output voltage of PNG was recorded at 30 Hz by using an electrodynamic shaker system.

Table S1 output performance comparison of PNGs based on PDMS.

Piezoelectric Materials	**Pressure (MPa)**	**V_{oc} (V)**	**J_{sc} (μA/cm^2)**	**Power density (μW/cm^2)**	**Growth Temper -ature**	**energy conversion efficiency**	**Ref.**
BCZT	0.085	28.8	0.6	N/A	high	N/A	1
$BaTiO_3$	0.002	2.7	0.26	0.12	high	N/A	2
$ZnSnO_3$	rolling tire	20	1	N/A	high	N/A	3
$BiFeO_3$	0.01	3	0.25	N/A	high	N/A	4
PMN-PT	tapping	7.8	4.6	N/A	high	N/A	5
Sm-PMN–PT	0.35	60	0.85	11.5	high	N/A	6
KNN-BNZ-AS-Fe	0.0625	52	1.2	N/A	high	N/A	7
$FAPbBr_3$	0.5	8.5	3.8	12	low	0.44%	8
$MAPb_xFe_{(1-x)}I_3$	0.5	7.3	0.88	N/A	low	N/A	9
$(ATHP)_2PbBr_2Cl_2$	4.66 kPa	74	6.5 μA	1.7	low	N/A	10
$FASnBr_3$	4.66kPa	94.5	19.1 μA	18.95	low	N/A	11
$CsPbBr_3$	**5.25kPa**	**50**	**5.5 μA**	**2.5**	**low**	**21.7%**	**This work**

[1] X. Gao, M. Zheng, X. Yan, J. Fu, M. Zhu and Y. Hou, J. Mater. Chem. C, 2019, 7, 961.

[2] J. Yan and Y. G. Jeong, ACS Appl. Mater. Interfaces, 2016, 8, 15700.

[3] K. Y. Lee, D. Kim, J.-H. Lee, T. Y. Kim, M. K. Gupta and S.-W. Kim, Adv. Funct. Mater., 2014, 24, 37.

[4] X. Ren, H. Fan, Y. Zhao and Z. Liu, ACS Appl. Mater. Interfaces, 2016, 8, 26190.

[5] S. Xu, Y. W. Yeh, G. Poirier, M. C. McAlpine, R. A. Register and N. Yao, Nano. Lett., 2013, 13, 2393.

[6] Y. Zhang, C. K. Jeong, J. Wang, H. Sun, F. Li, G. Zhang, L.-Q. Chen, S. Zhang, W. Chen and Q. Wang, Nano Energy, 2018, 50, 35.

[7] M. Wu, T. Zheng, H. Zheng, J. Li, W. Wang, M. Zhu, F. Li, G. Yue, Y. Gu and J. Wu, J. Mater. Chem. A, 2018, 6, 16439.

[8] R. Ding, H. Liu, X. Zhang, J. Xiao, R. Kishor, H. Sun, B. Zhu, G. Chen, F. Gao, X. Feng, J. Chen, X. Chen, X. Sun and Y. Zheng, Adv. Funct. Mater., 2016, 26, 7708.

[9] S. Ippili, V. Jella, J. Kim, S. Hong and S.-G. Yoon, Nano Energy, 2018, 49, 247.

[10] A. A. Khan, G. Huang, M. M. Rana, N. Mei, M. Biondi, S. Rassel, N. Tanguy, B. Sun, Z. Leonenko, N. Ying, C. Wang, S. Xu, D. Ban, *Nano energy,* 2021, 86, 106039.

[11] M. M. Rana, A. A. Khan, W. Zhu, M. F. A. Fattah, S. Kokilathasan, S. Rassel, R. Bernard, S. A. -Girard, P. Turban, S. Xu, C. Wang, D. Ban, *Nano energy,* 2022, 101, 107631.

[12] G. Huang, C. Wang, S. Xu, S. Zong, J. Lu, Z. Wang, C. Lu and Y. Cui, Advanced Materials, 2017, 29, 1700095.